

A Variational Approach to Hyperspectral Image Fusion

Michael Moeller^a, Todd Wittman^b, Andrea L. Bertozzi^b

^aWestfaelische Wilhelms Univ., Einsteinstrasse 62, 48149 Muenster, Germany

^bUniv. of California, 520 Portola Plaza, Los Angeles, CA 90095, USA

ABSTRACT

There has been significant research on pan-sharpening multispectral imagery with a high resolution image, but there has been little work extending the procedure to high dimensional hyperspectral imagery. We present a wavelet-based variational method for fusing a high resolution image and a hyperspectral image with an arbitrary number of bands. To ensure that the fused image can be used for tasks such as classification and detection, we explicitly enforce spectral coherence in the fusion process. This procedure produces images with both high spatial and spectral quality. We demonstrate this procedure on several AVIRIS and HYDICE images.

Keywords: image fusion, hyperspectral imagery, calculus of variations

1. INTRODUCTION

Hyperspectral imagery typically possesses high spectral resolution, but much lower spatial resolution than could be obtained with other types of sensors. The spectral signature of a single pixel gives useful information about the materials present in a specific location. However, the low spatial resolution makes it difficult to obtain common visual cues such as edges and shapes that would be determined by a group of pixels. One way to enhance the spatial resolution is to fuse the spectral information from the hyperspectral image and the spatial information obtained from a high resolution "master" image.

For low-dimensional (4-6 band) multispectral imagery, several methods have been proposed for fusing the multispectral image with a high resolution master image.¹⁻⁸ In satellites such as Landsat and Quickbird, this master image is a panchromatic image with high spatial resolution but low spectral resolution. This sharpening process is called image fusion or pan-sharpening.

Only a few methods for resolution enhancement of hyperspectral images have been proposed.^{9,10} Most pan-sharpening methods do not easily extend to high-dimensional data. In addition, most methods assume the master image spans the spectral responses of the multispectral bands. That is, the master image is assumed to be panchromatic. Given that hyperspectral images are typically obtained from low altitude aircraft and panchromatic images from orbiting satellites, it is difficult to find hyperspectral and panchromatic images for the same scene. Even if matching data is found, it is difficult to accurately align the images. Therefore, we wish to develop a method for which the high resolution master image is not assumed to be panchromatic.

Recently, the authors have proposed a method for enhancing multispectral imagery called Variational Wavelet Pan-sharpening (VWP).¹¹ This method was shown to be effective for enhancing the spatial resolution of multispectral images, while still maintaining the spectral information present in the original data. In this manuscript, we will show how VWP extends to hyperspectral imagery. We believe that VWP is better suited for sharpening hyperspectral imagery than classical pan-sharpening methods for the following three reasons.

- The VWP model can process images with an arbitrary number of spectral bands.
- VWP explicitly enforces spectral cohesion. At every pixel, the spectral signature in the sharpened image should resemble the signature present in the original data.

Send correspondence to Michael Moeller

Michael Moeller: michaelm@math.ucla.edu

Todd Wittman: wittman@math.ucla.edu

Andrea L. Bertozzi: bertozzi@math.ucla.edu

- VWP does not make any assumption on the spectral response of the master image. The master image does not need to be panchromatic, any high resolution grayscale image should suffice. For our experiments, our master image was taken from Google maps.

In this manuscript, we will show how VWP extends to hyperspectral imagery. We will first present the VWP energy and briefly describe its numerical implementation. We conclude by presenting sharpening results on AVIRIS and HYDICE data.

2. ENERGY FUNCTIONAL

The general idea of variational image processing methods is to develop an energy functional depending on an image, where a low value of the energy functional corresponds to a good quality image. A general description of variational image processing methods can be found in the book “Image Processing and Analysis” by Chan and Shen.¹²

The VWP energy functional we used for sharpening hyperspectral images was originally designed for pan-sharpening.¹¹ It consists of three parts and is specifically designed to sharpen images with an arbitrary number of bands while preserving spectral quality. In the following we describe each term of our energy functional separately. We refer to the master image as $M : \Omega \rightarrow \mathbb{R}$, where $\Omega \subset \mathbb{R}^2$ is the image domain. H_i are the original low resolution and u_i the desired high resolution hyperspectral bands.

2.1 Geometry enforcing term

Recently Ballester et al. proposed a variational pan-sharpening method where their idea for introducing the geometry of the panchromatic image was to align all level lines of the high resolution panchromatic and each multispectral band.⁸ Their main assumption was that the geometry of an image is contained in its level sets, independent of their actual level. These level sets are represented by the vector field θ consisting of all unit normal vectors to the level sets which can be calculated almost everywhere under certain general conditions. In practice the vector field is implemented as $\theta(x) = \frac{\nabla M(x)}{|\nabla M(x)|_\epsilon}$ where $|\nabla M|_\epsilon = \sqrt{(D_x M)^2 + (D_y M)^2 + \epsilon^2}$ is a regularization to avoid division by zero. The panchromatic master image M then satisfies $\theta \cdot \nabla M = |\nabla M|$. To ensure that each spectral band has the same level sets as the panchromatic image, Ballester et al. suggested to align the normal vectors of the level sets. Therefore, every band of the restored image should satisfy $|\nabla u_n| - \theta \cdot \nabla u_n = 0$.

This idea can easily be adapted for the sharpening of hyperspectral images with an arbitrary master image at high resolution. θ depends only on the level sets of the image and therefore no assumption on the relation between the hyperspectral image and the master image needs to be made.

We start the construction of our energy similarly to the P+XS model⁸ and just weight the two terms separately with parameter γ and η :

$$E_g = \sum_{n=1}^N [\gamma \int_{\Omega} |\nabla u_n| dx + \eta \int_{\Omega} \text{div}(\theta) \cdot u_n dx]. \quad (1)$$

This term does an excellent job enforcing spatial quality. Notice that the first part of this term is Total Variation (TV) regularization¹³ for each band. Furthermore, the idea of aligning the gradient vectors of an image with a smooth unit normal vector field was also proposed by Lysaker, Osher and Tai¹⁴ and led to iterative regularization using the Bregman distance.¹⁵

2.2 Fidelity term

We would like our final image to be very close to the low resolution image on those parts of the image, where there are no edges or texture. On the edges we would like to increase the contrast and enhance the spatial information. The original idea for VWP therefore is to include two terms, a wavelet term which matches the approximation coefficients (color information) of our current iteration to the approximation coefficients of each band of the low resolution image and the detail coefficients (edge information) to the detail coefficients of the master image¹¹ and, to ensure spectral quality, a matching term to the low resolution image away from the edges.

As described in the VWP paper,¹¹ this procedure is computationally expensive since it requires a wavelet transform and reconstruction every iteration in any minimization scheme. In very high dimensional imagery, this can lead to extremely long run times and even memory problems. For faster minimization we develop an alternate energy that incorporates the above ideas and allows minimization in the spatial domain only:

We match our current iteration to the low resolution image away from the edges and to a wavelet fused image on the edges. The wavelet fused image is obtained as shown in figure 1.

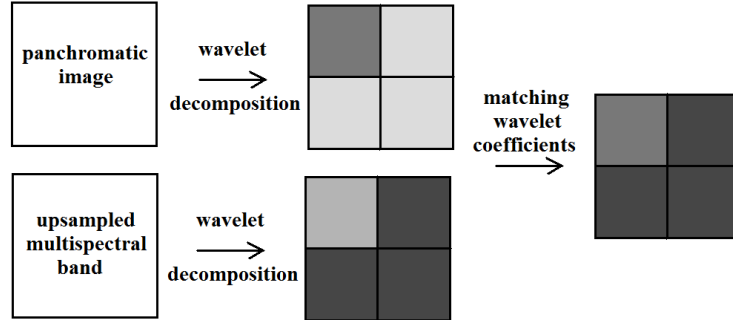


Figure 1. Sharpening of hyperspectral imagery - results displayed as false color images

A second level wavelet decomposition of the master image and each hyperspectral band is calculated and the matching image results from a wavelet reconstruction with the detail coefficients of the master image and the approximation coefficients of each band. This is a well known procedure for wavelet pan-sharpening.⁵ In our experiments we use Matlab’s “sym4” stationary wavelet decomposition. This choice is slower than the orthogonal transform, but gives much better fusion results.¹⁶⁻¹⁹

For the edge detection we use $\exp(-\frac{d}{|\nabla M|^2})$ which has successfully been used in many image processing applications such as the Perona-Malik model.²⁰ Denoting the wavelet fused image for the q^{th} band with W_q and the new matching image with Z_q we have

$$Z_q = \exp(-\frac{d}{|\nabla M|^2}) \cdot W_q + (1 - \exp(-\frac{d}{|\nabla M|^2})) \cdot \uparrow H_q, \quad (2)$$

where \uparrow denotes upsampling to the high resolution image size. We then force our result to match the fused image Z_q by adding the term

$$E_a = \nu \sum_{n=1}^N \int_{\Omega} (u_n - Z_n)^2 dx \quad (3)$$

to our energy.

2.3 Spectral correlation preserving term

So far we constrain the colors within each band and introduce the spatial information from the master image, but none of the terms couples the different bands. For hyperspectral imagery the spectral signature of each pixel is extremely important, because it can be used for material identification and classification tasks. Therefore, it is crucial to preserve the frequency information from the original low resolution hyperspectral image. Not changing the signature at all would of course allow no sharpening, but if we relax this constraint and just keep the signature vectors parallel, we can enhance edges and thereby increase the visual quality. We propose that every possible ratio of two different spectral bands of our sharpened image should equal the ratio of the same bands of the original hyperspectral image. Mathematically, this means that we would like to obtain

$\frac{u_i}{u_j} = \frac{\uparrow H_i}{\uparrow H_j} \Rightarrow u_i \cdot \uparrow H_j - u_j \cdot \uparrow H_i = 0$ at every pixel. Therefore, we add the sum of the squares of the corresponding L_2 norms to our energy functional:

$$E_s = \mu \sum_{i,j=1, i < j}^N \int_{\Omega} (u_i \cdot \uparrow H_j - u_j \cdot \uparrow H_i)^2 dx \quad (4)$$

For an arbitrary but fixed pixel let \vec{a} be the frequency vector in the low resolution and \vec{b} the frequency vector in the corresponding high resolution image. The minimizer of the above energy term is $a(i) \cdot b(j) - a(j) \cdot b(i) = 0 \forall i, j$. This can be rewritten as $a(i) = \frac{a(j)}{b(j)} \cdot b(i) = 0 \forall i, j$ which proves that $\vec{a} \parallel \vec{b}$. Notice that this means that the spectral angle $SAM = \arccos(\frac{\langle \vec{a}, \vec{b} \rangle}{\|\vec{a}\| \cdot \|\vec{b}\|})$ becomes zero and all classification methods based on SAM will give the same result on the sharpened image as they do on the original hyperspectral image.

Putting the terms (1), (3) and (4) together, the total energy functional we minimize is

$$E(u) = E_g + E_s + E_a. \quad (5)$$

To practically minimize this problem we make use of the necessary constraint for minima that the first variation of the energy functional must equal zero. For the q^{th} band we get:

$$\frac{\delta E_g}{\delta u_q} = -(\gamma \operatorname{div}(\frac{\nabla u_q}{|\nabla u_q|_\epsilon}) - \eta \operatorname{div}(\theta)) \quad (6)$$

$$\frac{\delta E_s}{\delta u_q} = 2\mu \sum_{j=1, j \neq q}^N (u_q \cdot \uparrow H_j - u_j \cdot \uparrow H_q) \uparrow H_j \quad (7)$$

$$\frac{\delta E_c}{\delta u_q} = 2\nu(u_q - Z_q) \quad (8)$$

We then apply a gradient descent method to

$$\frac{\delta E_g}{\delta u_q} + \frac{\delta E_s}{\delta u_q} + \frac{\delta E_c}{\delta u_q} = 0. \quad (9)$$

and solve the resulting PDE with an alternating directions implicit (ADI) method similar to the ideas of Douglas, Peaceman and Rachford.^{21,22} The details of this method can be found in our VWP paper.¹¹

Recently, Goldstein and Osher have developed a method called Split Bregman method for L_1 minimization problems,²³ which can be used to minimize the total variation energy very efficiently. The same technique can be applied to minimize our energy (5): The idea is to split the total variation term from the rest of the energy functional by introducing a new variable $d = \nabla u$ and optimize for u and d . For the sake of simplicity we just give the final algorithm and refer to the original Split Bregman paper²³ for more details on the derivation.

The algorithm works as follows. While the residual per pixel in the current iteration $\frac{\|u^{k+1} - u^k\|_1}{\operatorname{size}(u)}$ is above a certain threshold, we perform three minimization steps for each band u_q .

1. We solve the linear equation

$$(2\nu + 2\mu \sum_{j=1, j \neq q}^N (\uparrow H_j)^2 - \lambda \Delta) u_q^{k+1} = 2\nu Z_q + \eta \operatorname{div}(\theta) + 2\mu \uparrow H_q (\sum_{j=1, j \neq q}^N u_j^{k*} \cdot \uparrow H_j) - \lambda \operatorname{div}(d_q^k - b_q^k) \quad (10)$$

approximately by one step of a Gauss-Seidel algorithm. Notice that we decoupled the bands by using $u_j^{k*} = u_j^{k+1}$ for $j < q$ and $u_j^{k*} = u_j^k$ for $j > q$ on the right hand side of the equation.

2. Secondly, we solve the minimization for d by shrinkage

$$(d_q^{k+1})_x = \max(s^k - 1/\lambda, 0) \frac{\nabla_x u_q^{k+1} + (b_q^k)_x}{s^k} \quad (11)$$

$$(d_q^{k+1})_y = \max(s^k - 1/\lambda, 0) \frac{\nabla_y u_q^{k+1} + (b_q^k)_y}{s^k} \quad (12)$$

with $s^k = \sqrt{|\nabla_x u_q^{k+1} + (b_q^k)_x|^2 + |\nabla_y u_q^{k+1} + (b_q^k)_y|^2}$.

3. Finally, we update the variable b_q by

$$(b_q^{k+1})_x = (b_q^k)_x + (\nabla_x u_q^{k+1} - (d_q^{k+1})_x) \quad (13)$$

$$(b_q^{k+1})_y = (b_q^k)_y + (\nabla_y u_q^{k+1} - (d_q^{k+1})_y) \quad (14)$$

and iterate these three steps until the stopping condition is met.

3. NUMERICAL RESULTS

We work with two datasets: An 82-band AVIRIS hyperspectral image of San Diego Harbor and a 210 band HYDICE hyperspectral image of an urban scene in Texas which is freely available online.²⁴ Since we do not have a master image, we looked at the same scene on Google MapsTM²⁵ (which offers very high resolution images) and extracted several scenes as our master images. The hyperspectral images are spatially distorted in comparison to the Google MapsTM image and therefore registration is needed. For the examples shown in this report we did the registration on small parts of the image manually.

Results of sharpening hyperspectral images are shown in figures 3, 4 and 5. The choice of parameter we used is $\gamma = 1$, $\eta = 1$, $\nu = 2$, $\mu = 300$ and $\epsilon = 5 \cdot 10^{(-2)}$ for the ADI method and $\gamma = 1$, $\eta = 1$, $\nu = 2$, $\mu = 500$ and $\epsilon = 5 \cdot 10^{(-4)}$ for the Split Bregman method. Notice, that the Split Bregman method needs the additional regularization parameter ϵ only for calculating θ and not for the total variation term which leads to a more precise minimization of our energy functional. To sharpen a hyperspectral image of 345 x 276 pixel with 82 bands the ADI method takes about 7 minutes and 46 seconds, and the Split Bregman method about 6 minutes and 11 seconds to converge on an Intel Duo Core processor with 2GHz and 3GB memory. The two different minimization methods give visually undistinguishable results, such that we only present one sharpened image per testimage.

The first example is taken from the urban scene in Texas. Figure 2 shows the whole image where the red rectangle marks the part of the image we selected for the sharpening process.



Figure 2. Selected scene of the Urban image - displayed as false a color image

We look up the exact same scene on Google MapsTM and extract a master image for the sharpening. Figure 3 shows the master image, the low resolution image and the sharpened image.

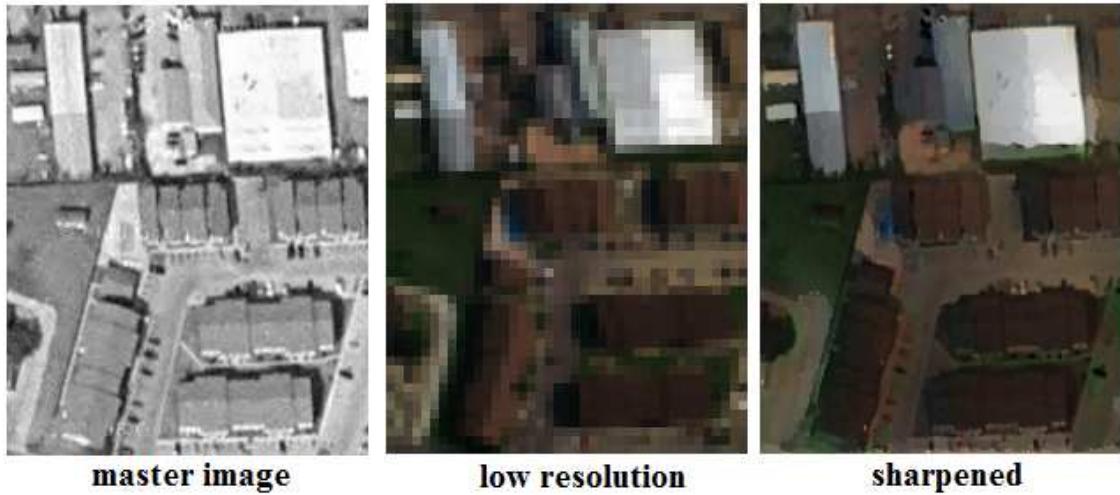


Figure 3. left image: master image ‘©2009 Google - Imagery ©2009 DigitalGlobe, Sanborn, Cnes/Spot Image GeoEye, U.S. Geological Survey’; middle and right image: low resolution and sharpened image

The visual quality greatly improves. The blocky low resolution image becomes a much smoother image with sharp edges in which a lot of spatial details from the master image can be seen. In a few regions some colors flow over certain edges which is due to a slightly inaccurate registration. Nevertheless, we gain a lot of spatial quality through the sharpening process.

The increase in resolution is even more dramatic for the San Diego harbor image for which Google Maps™ allows an even higher zoom. Figure 4 shows a building with some boxes in front of it. In the low resolution hyperspectral image we can see that there is something in front of the building, but the identification of the actual object (and its shape) is impossible even if we had the material information from analyzing the hyperspectral bands. In the sharpened image we can clearly see the shape of the objects and identify them as boxes or containers.

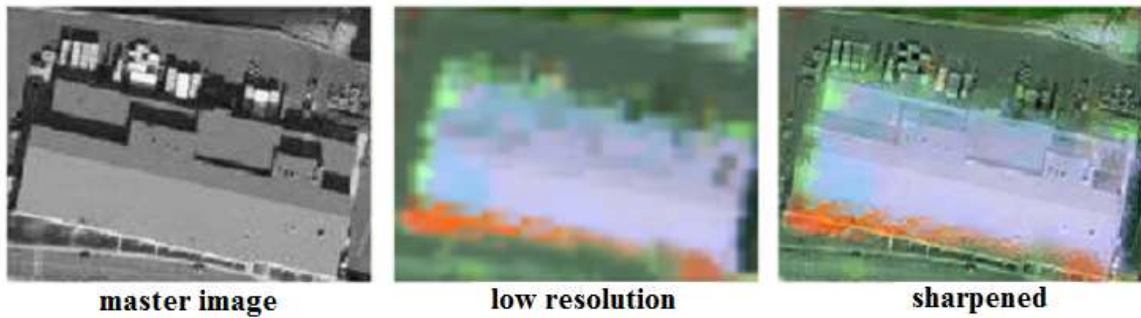


Figure 4. left image: master image ‘©2009 Google - Imagery ©2009 DigitalGlobe, GeoEye’; middle and right image: low resolution and sharpened image displayed as false color images

In figure 5 we see the top of a building and the master image shows that there are some pipes on the roof, probably from an air conditioning system. The hyperspectral image itself is much too blurry for this detail and an analysis of this image would probably only indicate that there is a certain amount of metal on the roof. Only the sharpened image contains both pieces of information: the shape and the spectral signature of the material of the pipes.



Figure 5. left image: master image ‘©2009 Google - Imagery ©2009 DigitalGlobe, GeoEye’; middle and right image: low resolution and sharpened image displayed as false color images

In general we can say that the visual quality is greatly increased by the sharpening process. While in the low resolution hyperspectral images small objects can almost not be visually identified, the sharpened images are very close to the master images in terms of spatial quality.

We should mention that we do not know when the Google Maps™ picture was taken. The boxes in figure 4 for instance could be things we see in the master image that were not present in the hyperspectral image and therefore appear as phantoms. One has to be careful with the introduced spatial information, if the two images were not taken at the same time. On the other hand, this could also be a chance because high resolution satellite images are much easier to obtain than hyperspectral images. One could visually update an older hyperspectral image with the spatial information of a recent master image.

As mentioned earlier the most important issue in sharpening hyperspectral images is that the spectral signature of each pixel is preserved since this information is used for material classification. To investigate how the spectral signature changes during the sharpening process we select three pixels in the 82 band hyperspectral scene and look at their spectral signature. Figure 6 shows the result of the sharpening process as well as the 3 pixels we selected to examine the change of spectral response during the sharpening process.

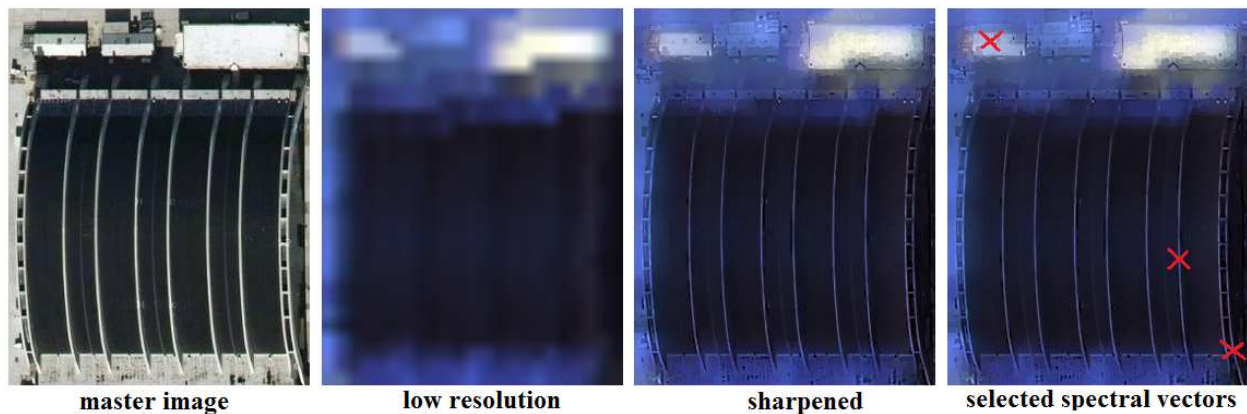


Figure 6. left image: master image ‘©2009 Google - Imagery ©2009 DigitalGlobe, GeoEye’; middle left and middle right image: low resolution and sharpened image displayed as false color images; right image: pixels to investigate the spectral signature of, we will refer to these pixel as pixel (1), (2) and (3) from left to right.

Pixel (1) is in the middle of a box where there are no edges or texture even in the master image. At these pixels we match our current iteration to the low resolution image and therefore do not change the intensity in any band. Indeed the comparison of the spectral signatures between the low resolution image and the sharpened image at that point is almost identical as shown in figure 7.

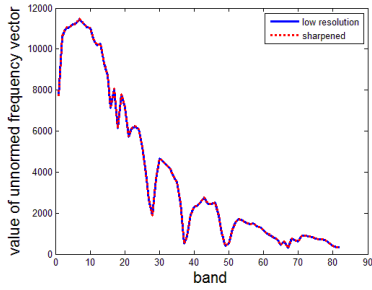


Figure 7. Spectral response of pixel (1)

At pixel (2) and (3) we are sure to change the signature because we want to increase the contrast at these points to enhance the edges. Looking at figure 8 we can clearly see this change in contrast.

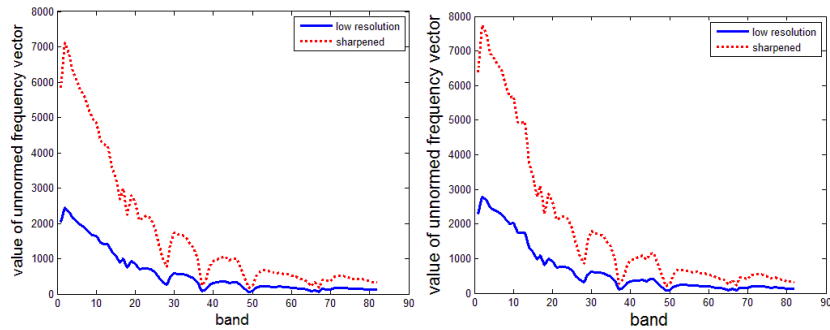


Figure 8. Spectral response of pixel (2) and (3)

Our energy model allows this increase of contrast, but enforces the frequency vectors to stay parallel. In other words, we keep the spectral angle at 0 degrees. If we normalize both spectral responses to have Euclidean norm 1 we get the result shown in figure 9.

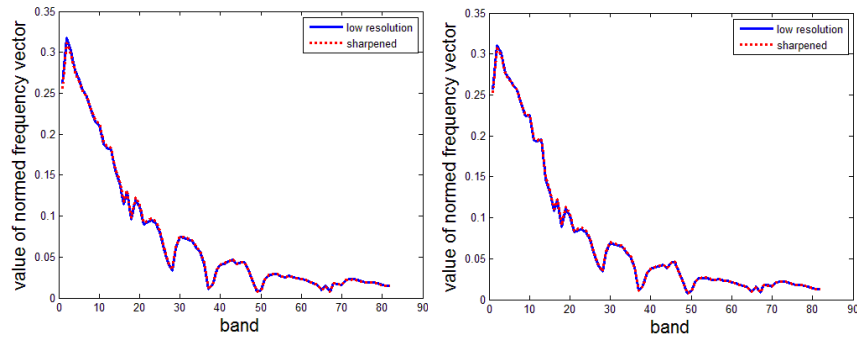


Figure 9. Normed spectral response of pixel (2) and (3)

The spectral responses match almost perfectly for both pixel. The frequency vectors stay parallel such that any classification or identification method using the spectral angle will give exactly the same result on the spatially enhanced image as it would on the low resolution version. To ensure, that this observation is true independent of the testpixels we choose, we calculated the average change in spectral angle for all frequency vectors in the whole image and found the change to be less than 1 degree.

4. CONCLUSIONS

We proposed a variational method for sharpening hyperspectral images which extends the VWP model from pan-sharpening to an arbitrary number of bands with a master image that does not need to be panchromatic. The energy model incorporates the alignment of all unit normal vectors of the level sets of each band with the master image and uses a fidelity term with a combination of the original and a wavelet fused hyperspectral image. By keeping the ratio of all bands constant we assure spectral quality. Large weights on this spectral quality term force the spectral angle between the original and the sharpened hyperspectral image to be close to zero.

Among all pan-sharpening methods VWP is the only method that easily extends to hyperspectral imagery while preserving the spectral information. Any material classification method that uses the normed spectral response vectors will do equally well on the sharpened image as on the original image, while an analyst's work is greatly simplified by the additional spatial information.

For future research one could try to incorporate technical information about the satellite sensors into the variational framework and other types of sensors and images could be used. To automate the sharpening process a robust registration method is needed. To reduce the bleeding of colors over some of the edges, deblurring could be included in the sharpening method. Furthermore, this method could be combined with hyperspectral analysis methods like demixing to not only improve the spatial but also the spectral resolution of the image. New detection and classification methods especially suitable for sharpened images could be developed, which take the spectral as well as the spatial information into account.

ACKNOWLEDGMENTS

The authors would like to thank Tom Goldstein, Stanley Osher, Julia Dobrosotskaya, Jerome Darbon, Ernest Esser, Luminata Vese and Martin Burger for their advice. This work was supported by the US Department of Defense, ONR grant N000140810363, NSF grant ACI-0321917 and NSF grant DMS-0601395.

REFERENCES

1. M. Choi, H.-C. Kim, N. Cho, and H. O. Kim, "An Improved Intensity-Hue-Saturation Method for IKONOS Image Fusion," *submitted to IJRS*.
2. M. Choi, "A New Intensity-Hue-Saturation Fusion Approach to Image Fusion with a Tradeoff Parameter," *IEEE Trans. on Geosci. and Remote Sens.* **44**, pp. 1672–1682, 2006.
3. Q. Du, N. Younan, R. King, and V. Shah, "On the performance evaluation of pan-sharpening techniques," *IEEE Geosci. and Remote Sens. Lett.* **4**, pp. 518–522, October 2007.
4. V. K. Shettigara, "A generalized component substitution technique for spatial enhancement of multispectral images using a higher resolution data set," *Photogrammetric eng. and remote sens.* **58**(5), pp. 561–567, 1992.
5. J. Zhou, D. L. Civico, and J. A. Silander, "A wavelet transform method to merge Landsat TM and SPOT panchromatic data," *Int. J. of Remote Sens.* **19**(4), 1998.
6. R. King and J. Wang, "A wavelet based algorithm for pan sharpening landsat 7 imagery," *Geosci. and Remote Sens. Symp., 2001. IGARSS '01. IEEE 2001 Int.* **2**, pp. 849–851, 2001.
7. N. Memarsadeghi, J. Le Moigne, and D. Mount, "Image fusion using cokriging," *Geosci. and Remote Sens. Symp., 2006. IGARSS 2006. IEEE Int. Conf. on*, pp. 2518–2521, August 2006.
8. C. Ballester, V. Caselles, L. Igual, and J. Verdera, "A Variational Model for P+XS Image Fusion," *Int. J. of Comput. Vision* **69**, pp. 43–58, August 2006.
9. R. C. Hardie, M. T. Eismann, and G. L. Wilson, "Map estimation for hyperspectral image resolution enhancement using an auxiliary sensor," *IEEE Trans. on Image Proc.* **13**, September 2004.
10. M. Winter, E. Winter, S. Beaven, and A. Ratkowski, "Hyperspectral image sharpening using multispectral data," *Aerospace Conference, 2007 IEEE*, pp. 1–9, March 2007.
11. M. Moeller, T. Wittman, and A. L. Bertozzi, "Variational Wavelet Pan-sharpening." *submitted to IEEE Trans. on Geosci. and Remote Sens.* for review, 12/19/08.
12. T. F. Chan and J. Shen, *Image Processing and Analysis*, SIAM, 2005.

13. L. I. Rudin, S. Osher, and E. Fatemi, "Nonlinear Total Variation Based Noise Removal Algorithms," *Physica D* **60**, pp. 259–268, November 1992.
14. O. Lysaker, S. Osher, and X.-C. Tai, "Noise removal using smoothed normals and surface fitting," *IEEE Trans. on Image Process.* **13**(10), pp. 1345–1357, 2004.
15. S. Osher, M. Burger, D. Goldfarb, J. Xu, and W. Yin, "An iterative regularization method for total variation-based image restoration," *SIAM Multiscale Modeling and Simulation* **4**, pp. 460–489, 2005.
16. Y. Chibani and A. Houacine, "Redundant versus orthogonal wavelet decomposition for multisensor image fusion," *Pattern Recognition* **36**, pp. 879–887, April 2002.
17. X. Otazu, M. Gonzalez-Audicana, O. Fors, and J. Nez, "Introduction of Sensor Spectral Response Into Image Fusion Methods. Application to Wavelet-Based Methods," *IEEE Trans. on Geosci. and Remote Sens.* **43**, October 2005.
18. G. Hong and Y. Zhang, "The Effects of Different Types of Wavelets on Image Fusion," *Proc. Int. Conf. on Image Process.* **3**, pp. 248 – 251, October 1995.
19. B. Aiazzi, L. Alparone, S. Baronti, and A. Garzelli, "Context-driven fusion of high spatial and spectral resolution images based on oversampled multiresolution analysis," *IEEE Trans. on Geosci. and Remote Sens.* **40**, pp. 2300 – 2312, 2002.
20. P. Perona and J. Malik, "Scale-space and edge detection using anisotropic diffusion," *IEEE Trans. Pattern Anal. Mach. Intell.* **12**, pp. 629–639, July 1990.
21. D. W. Peaceman and J. H. H. Rachford, "The numerical solution of parabolic and elliptic differential equations," *J. of the Soc. for Ind. and Applied Math.* **3**(1), pp. 28–41, 1955.
22. D. W. P. Jim Douglas Jr., "Numerical solution of two-dimensional heat-flow problems," *AICHE Journal* **1**(4), pp. 505–512, 1955.
23. T. Golstein and S. Osher, "The split bregman algorithm for l1 regularized problems," *UCLA CAM report* **08-29**, 2008.
24. US Army Corps Engineers, Online: <http://www.tec.army.mil/Hypercube/>.
25. Google, Inc., Google Maps. Online: <http://maps.google.com>, Jan. 2009.